Journal of Solid State Chemistry 182 (2009) 2887–2889

Contents lists available at ScienceDirect

Journal of Solid State Chemistry

journal homepage: www.elsevier.com/locate/jssc

Epitaxial growth of high purity cubic InN films on MgO substrates using HfN buffer layers by pulsed laser deposition

R. Ohba [a], J. Ohta [b,c], K. Shimomoto [b], T. Fujii [b], K. Okamoto [b], A. Aoyama [b], T. Nakano [c], A. Kobayashi [c], H. Fujioka [b,c,d,*], M. Oshima [a,d]

[a] Department of Applied Chemistry, The University of Tokyo, Hongo, Tokyo 113-8656, Japan
[b] Institute of Industrial Science (IIS), The University of Tokyo, Komaba, Tokyo 153-8505, Japan
[c] Kanagawa Academy of Science and Technology (KAST), Sakado, Kanagawa 213-0012, Japan
[d] Core Research for Evolutional Science and Technology (CREST), Japan Science and Technology Agency (JST), Chiyoda-ku, Tokyo 102-0075, Japan

ARTICLE INFO

Article history:
Received 21 April 2009
Received in revised form
30 July 2009
Accepted 1 August 2009
Available online 8 August 2009

Keywords:
Cubic InN
HfN
Pulsed laser deposition

ABSTRACT

Cubic InN films have been grown on MgO substrates with HfN buffer layers by pulsed laser deposition (PLD). It has been found that the use of HfN (100) buffer layers allows us to grow cubic InN (100) films with an in-plane epitaxial relationship of $[001]_{InN}//[001]_{HfN}//[001]_{MgO}$. X-ray diffraction and electron back-scattered diffraction measurements have revealed that the phase purity of the cubic InN films was as high as 99%, which can be attributed to the use of HfN buffer layers and the enhanced surface migration of the film precursors by the use of PLD.

InN has attracted much attention due to its excellent optical and electrical properties, which make it particularly suitable for the fabrication of IR optical devices and high speed electronic devices [1,2]. Although most research papers so far have dealt with hexagonal InN films, (which is the most stable phase of InN), metastable cubic InN theoretically possesses several advantages, such as higher electron mobility and improved doping efficiency [3–5]. An additional advantage for the use of cubic group III nitride (100) films is the elimination of the internal electric field that is induced by spontaneous and piezoelectric polarizations, which can be quite severe in the case of hexagonal InN (0001) [6]. Since advantages make cubic InN quite attractive, the epitaxial growth of cubic InN films has been recently tested on various substrates such as sapphire, GaAs, 3C–SiC, MgO and YSZ by molecular beam epitaxy (MBE) and by metal-organic vapor phase epitaxy (MOVPE) [4,5,7–11]. However, there are two serious problems which affect the growth of cubic InN films. One is the inclusion of the hexagonal phase. Cubic InN films can suffer from a high-density of crystalline defects such as stacking faults due to the formation of the hexagonal phase at the (111) facets of the cubic crystal. To avoid the inclusion of the hexagonal phase, the development of a growth technique that can enhance the surface migration of the film precursors is highly sought after. Recently, pulsed laser deposition (PLD), in which film precursors have high kinetic energies induced by laser ablation, has been recognized as a suitable technique for the growth of high-quality group III nitride films [12–16]. In fact, it has been reported that the PLD technique enables us to enhance the surface migration of film precursors and to grow group III nitride films epitaxially even at room temperature in the 'layer-by-layer' mode.

The other problem with the growth of cubic InN is the large lattice mismatch that occurs between cubic InN films and the available substrates. It is well known that a large lattice mismatch can often cause the formation of high-density crystalline defects such as misfit dislocations at the interface. In order to alleviate this problem, the insertion of a buffer layer that has an intermediate lattice constant between InN ($a = 0.498$ nm) and the substrate is desirable. Since we utilized MgO (100) ($a = 0.421$ nm) substrates in this study, then HfN ($a = 0.452$ nm), which has the 'rock-salt' crystalline structure, is an ideal material for this purpose. In addition, HfN has excellent physical properties, such as high thermal stability, high reflectivity, and high electrical conductivity ($\rho < 20\,\mu\Omega\,cm$) [17–19]. These features make HfN all the more attractive as a potential buffer layer for the growth of cubic InN (100) on MgO (100) substrates. In this letter, we report on the growth of cubic InN films on MgO (100) substrates with HfN buffer layers by PLD.

HfN buffer layers and InN films were grown using ultra-high vacuum pulsed sputtering deposition (PSD) and PLD systems,

* Corresponding author at: Institute of Industrial Science (IIS), The University of Tokyo, Komaba, Tokyo 153-8505, Japan.
E-mail address: hfujioka@iis.u-tokyo.ac.jp (H. Fujioka).

0022-4596/$ - see front matter © 2009 Elsevier Inc. All rights reserved.
doi:10.1016/j.jssc.2009.08.002

respectively. The PSD chamber for the growth of the HfN was equipped with a Hf metal (99.99% purity excluding Zr) target, while the PLD chamber was equipped with an In metal (99.9999% purity) target and a radio-frequency (rf) plasma generator. An MgO (100) substrate was loaded into the PSD chamber at a background pressure of 7×10^{-8} Pa. HfN buffer layers of 200 nm thickness were then grown on the MgO substrates by pulsed sputtering of the Hf target in an Ar/N_2 gas mixture for 40 min. The substrate temperature and the total gas pressure during the growth of the HfN were set at 1000 °C and 0.5 Pa, respectively. After the growth of the HfN layer, the samples were transferred into the UHV–PLD chamber for the growth of the InN layers. A KrF excimer laser ($\lambda = 248$ nm, $\tau = 20$ ns) was used to ablate an In target (99.9999%) with an energy density of approximately 3.0 J/cm^2 and with pulse repetition rates of between 1 and 10 Hz. During the growth of the films, a nitrogen plasma was supplied through an RF generator operating at 320 W. The substrate temperature was varied from 390 to 430 °C, and the thickness of the cubic InN films was set at 100 nm. The structural properties of the samples, including their crystalline quality and orientation relationships, were characterized by reflection high-energy electron diffraction (RHEED), X-ray diffraction (XRD) using a Rigaku ATX-G diffractometer, and electron back-scattered diffraction (EBSD) in an Oxford Instruments INCA Crystal EBSD system attached to a field-emission scanning electron microscope (JEOL JSM-6500F) operated at 20 kV. The purity of the cubic phase in the grown films was measured by conventional reciprocal space mapping (RSM) by XRD [20], and the phase mapping was implemented by scanning Kikuchi pattern identification from EBSD [21], which provides information on the phase distribution for the topmost 50 nm of the cubic InN films.

Fig. 1 shows a typical XRD curve for a HfN film grown at 1000 °C on an MgO (100) substrate. The strong peak at 39.7° was assigned to the HfN 2 0 0 diffraction, and the full-width at half-maximum (FWHM) value for the 200 rocking curve for this sample was as low as 33.6 arcmin. The superimposed image of Fig. 1 shows the RHEED patterns for the HfN buffer layers with an electron beam incidence parallel to HfN [001]. AFM observations for the HfN surfaces with an area of $2 \times 2\ \mu m^2$ have revealed that the root-mean-square (rms) value of the surface profile was as small as 0.5 nm. These results indicate that high quality HfN (100) can be grown on MgO (100) by the use of PSD. The growth of the InN films was then performed on these HfN (100) buffer layers. The RHEED patterns for InN films grown at 420 °C on MgO (100) substrates with a HfN buffer layer exhibited clear diffraction spots from cubic InN (100) with an electron beam incidence parallel to InN [001], as shown in Fig. 2(a). We have taken the RHEED images for HfN and InN while keeping the direction of incidence electron beam and found that the in-plane alignment between the films and MgO substrates is $[001]_{InN}//[001]_{HfN}//[001]_{MgO}$. This alignment is the expected one, in which the HfN buffer layer alleviates the lattice mismatch between the cubic InN and the MgO. The EBSD pole figure for InN {100} exhibited diffraction spots with clear four-fold rotational symmetry, as shown in Fig. 2(b). These results indicate that cubic InN (100) films can be grown epitaxially on MgO (100) substrates by using HfN (100) buffer layers in conjunction with the PLD technique. Fig. 2(c) shows an XRD $2\theta/\omega$ curve for a cubic InN film grown with a HfN buffer layer. The peaks that were observed at 35.6°, 39.7°, and 42.9° have been identified as the diffractions from cubic InN 2 0 0, HfN 2 0 0, and MgO 2 0 0, respectively. The lattice parameter of the cubic InN film was calculated to be 0.502 nm from the XRD measurements, which is in good agreement with the reported value [9]. This result indicates that the lattice strain in the cubic InN film is almost released. The FWHM value of the ω-scan rocking curve for the InN 2 0 0 diffraction was 51 arcmin. Fig. 2(d) shows an SEM image for an InN film grown at 420 °C on an MgO (100) substrate with a HfN buffer layer. One can clearly see square-shaped grains at the surface, and AFM observations for the InN surfaces with an area of $2 \times 2\ \mu m^2$ have revealed that the rms value of the surface profile was 4.1 nm. It is interesting to note that the direct growth of InN on MgO (100) without using a HfN buffer layer results in the formation of hexagonal InN (0001) with two equivalent in-plane 30°-rotational domains that have alignments of $[10\bar{1}0]_{InN}//[010]_{MgO}$ and $[10\bar{1}0]_{InN}//[001]_{MgO}$ [22]. The lattice mismatch between InN (0001) and MgO (100) is as low as 3% for these in-plane alignments. Since the lattice mismatch for InN (100)/MgO (100) is much larger (18%) than that for InN (0001)/MgO (100), it is reasonable to believe that the development of hexagonal InN growth with 30°-rotational domains is energetically favorable in the case of the direct growth of InN films on MgO (100). This observation indicates that the use of a HfN buffer layer is inherently important in order to obtain cubic InN.

To investigate the phase purity of the 100-nm-thick cubic InN films, EBSD phase-mapping and reciprocal space mapping (RSM) based on XRD measurements were performed. Fig. 3 shows the

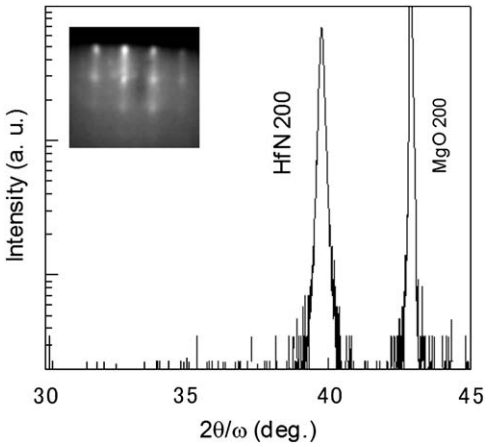

Fig. 1. XRD $2\theta/\omega$ scan for a HfN buffer layer grown on a MgO (100) substrate. Superimposed image shows a RHEED pattern for HfN with an electron beam incidence parallel to HfN [001].

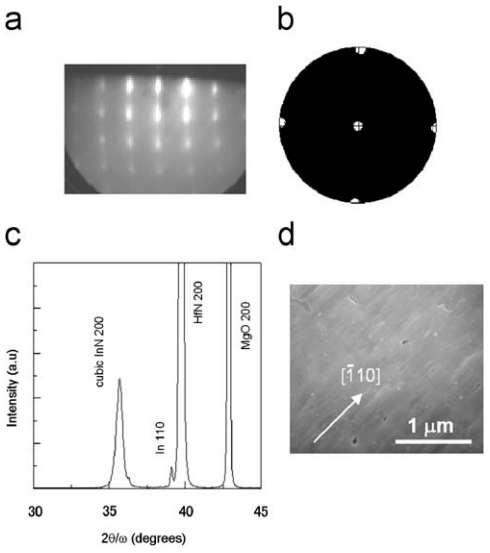

Fig. 2. (a) RHEED pattern for cubic InN grown on the HfN/MgO structure with the electron beam incidence parallel to InN [001], (b) EBSD pole figure, (c) XRD $2\theta/\omega$ scan, and (d) SEM image for cubic InN grown on the HfN/MgO structure.

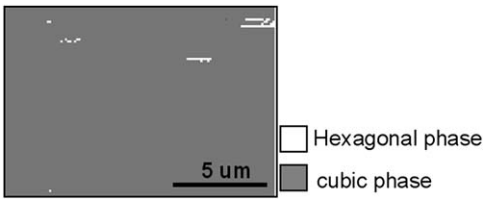

Fig. 3. Phase mapping for InN by scanning Kikuchi pattern identification of EBSD measurements.

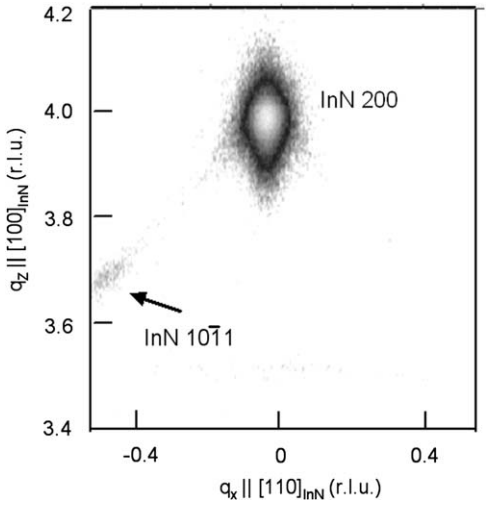

Fig. 4. XRD RSM for the cubic InN films grown on MgO (100) with HfN buffer layers.

results of EBSD phase-mapping for a cubic InN film, and it was found that the phase purity of the film was as high as 99%. It should be noted that this cubic-phase purity is quite high compared with the reported values of around 95% that have been obtained by other growth techniques [4,9]. We believe that the formation of high phase purity InN can be attributed to enhancement in the surface migration of the film precursors induced by the use of PLD, which helps to convey the crystalline information from the substrate to the film. Fig. 4 shows the result of RSM for a cubic InN film. Although two diffraction spots for hexagonal InN {10$\bar{1}$1} were expected to appear on the RSM in addition to the cubic InN 2 0 0, only one spot was observed. This result indicates the anisotropic inclusion of the hexagonal phase in the cubic InN (100) film. An EBSD pole figure for hexagonal InN {0001} showed a two-fold rotational symmetry, which well agrees with the results from the RSM measurements. This phenomena can be explained by the fact that the hexagonal phase tends to be incorporated in the cubic phase through the incidental stacking faults on the cubic InN {111}B planes rather than the {111}A planes [7]. From the integrated intensities of the diffraction peaks for the hexagonal and cubic phases of InN, the phase purity of cubic InN was calculated to be about 99%, which coincides with the EBSD results.

In conclusion, we have grown InN (100) on MgO (100) substrates by PLD, and we found that the use of a PSD-grown HfN buffer layer prior to the growth of the InN allowed us to grow cubic InN (100) films with an in-plane epitaxial relationship of $[001]_{InN}//[001]_{HfN}//[001]_{MgO}$. XRD and EBSD measurements have revealed that the phase purity of the cubic InN films was as high as 99%. This high value suggests that the use of PLD suppresses the formation of nucleation centers for the hexagonal phase in the cubic InN films by enhancing the effects of surface migration. These results indicate that the use of PLD and HfN buffer layers is quite promising for the production of future long-wavelength optical devices and high-speed electron devices based on cubic InN.

References

[1] Y. Nanishi, Y. Saito, T. Yamaguchi, Jpn. J. Appl. Phys. 42 (2003) 2549.
[2] K. Xu, A. Yoshikawa, Appl. Phys. Lett. 83 (2003) 251.
[3] S. Yoshida, Physica E 7 (2000) 907.
[4] T. Nakamura, Y. Tokumoto, R. Katayama, T. Yamamoto, K. Onabe, J. Cryst. Growth 301–302 (2007) 508.
[5] K. Nishida, Y. Kitamura, Y. Hijikata, H. Yaguchi, S. Yoshida, Phys. Status Solidi (b) 241 (2004) 2839.
[6] S.F. Chichibu, T. Onuma, T. Aoyama, K. Nakajima, P. Ahmet, T. Chikyow, T. Sota, S.P. DenBaars, S. Nakamura, T. Kitamura, Y. Ishida, H. Okumura, J. Vac. Sci. Technol. B 21 (2003) 1856.
[7] T. Nakamura, K. Iida, R. Kitayama, T. Yamamoto, K. Onabe, Phys. Status Solidi (b) 243 (2006) 1451.
[8] V. Cimalla, J. Pezoldt, G. Ecke, R. Kosiba, O. Ambacher, L. Spieβ, G. Teichert, H. Lu, W.J. Schaff, Appl. Phys. Lett. 83 (2003) 3468.
[9] Y. Iwahashi, H. Yaguchi, A. Nishimoto, M. Orihara, Y. Hijikata, S. Yoshida, Phys. Status. Solidi (c) 3 (2006) 1515.
[10] J.G. Lozano, F.M. Morales, R. García, D. González, V. Lebedev, Ch.Y. Wang, V. Cimalla, O. Ambacher, Appl. Phys. Lett. 90 (2007) 091901.
[11] J. Schörmann, D.J. As, K. Lischka, P. Schley, R. Goldhahn, S.F. Li, W. Löffler, M. Hetterich, H. Kalt, Appl. Phys. Lett. 89 (2006) 261903.
[12] M.H. Kim, J. Ohta, A. Kobayashi, H. Fujioka, M. Oshima, Appl. Phys. Lett. 91 (2007) 151903.
[13] K. Ueno, A. Kobayashi, J. Ohta, H. Fujioka, Jpn. J. Appl. Phys. 45 (2006) L1139.
[14] S. Inoue, K. Okamoto, N. Matsuki, T.-W. Kim, H. Fujioka, Appl. Phys. Lett. 88 (2006) 261910.
[15] T. Honke, H. Fujioka, J. Ohta, M. Oshima, J. Vac. Sci. Technol. A 22 (2004) 2487.
[16] A. Kobayashi, J. Ohta, H. Fujioka, Jpn. J. Appl. Phys. 45 (2006) L611.
[17] H.-S. Seo, T.-Y. Lee, J.G. Wen, I. Petrov, J.E. Greene, D. Gall, J. Appl. Phys. 96 (2004) 1.
[18] H.-S. Seo, I. Petrov, J.E. Greene, J. Appl. Phys. 99 (2006) 043507.
[19] L. Yuan, G. Fang, C. Li, M. Wang, N. Liu, L. Ai, Y. Cheng, H. Gao, X. Zhao, Appl. Surf. Sci. 253 (2007) 8538.
[20] B. Qu, X.H. Zheng, Y.T. Wang, Z.H. Feng, S.A. Liu, S.M. Lin, H. Yang, J.W. Liang, Thin Solid Films 392 (2001) 29.
[21] C. Trager-Cowan, F. Sweeney, A.J. Wilkinson, I.M. Watson, P.G. Middleton, K.P. O'Donnell, D. Zubia, S.D. Hersee, S. Einfeldt, D. Hommel, Phys. Status Solidi (c) 0 (2002) 532.
[22] R. Ohba, K. Mitamura, K. Shimomoto, T. Fujii, S. Kawano, J. Ohta, H. Fujioka, M. Oshima, J. Cryst. Growth 311 (2009) 3130.